Preprints of the 19th World Congress
The International Federation of Automatic Control
Cape Town, South Africa. August 24-29, 2014

Passive Phase Design of a Pumping Kite Wind Generator ⋆

Ramiro Saraiva * **Marcelo De Lellis** ** **Alexandre Trofino** ***

Department of Automation and Systems, Federal University of Santa Catarina, ZIP 88040-900, PO box 476, Florianópolis, Brazil.
* *ramiro.saraiva@posgrad.ufsc.br*
** *marcelo.lellis@posgrad.ufsc.br*
*** *alexandre.trofino@ufsc.br*

Abstract:
In this paper, the passive phase of a pumping kite wind generator is designed. A robustness index against wind turbulence is proposed and analyzed, and an offline algorithm for generating a flight trajectory reference, which maximizes the cycle power while considering a desired robustness index, is presented. Based on a given tracking controller, simulation results are discussed.

1. INTRODUCTION

According to the International Energy Agency [2012], renewable energy sources are expected to account for almost one-third of the total world electricity output by the year 2035. Among them, wind power offers advantages like having a low environmental impact, and being an excellent supplement to other energy sources.

Archer et al. [2014] showed that, since the wind power depends on the cube of the wind speed, which usually increases with altitude, High-Altitude Wind Energy (HAWE) is an abundant energy source highly available worldwide. However, it cannot be harnessed by conventional wind turbines because their use is technically and economically viable only in altitudes up to 150 m. Given that no breakthrough in the current technology is expected, Airborne Wind Energy (AWE) offers a new approach to exploit HAWE at a competitive cost.

Tethered airfoils, also known as power kites, have been investigated in the last decade as an AWE alternative to the wind turbines. Ahmed et al. [2012] and Ahrens et al. [2013] made a comprehensive overview of the configurations of such systems proposed thus far. The majority of the studies found in the literature addresses the *pumping kite* (*yoyo*) configuration, which employs a single kite. Electric power is obtained by unwinding a tether from a drum [1] connected to a generator/motor on the ground.

Houska and Diehl [2007] investigated a pumping kite flying closed orbits, in which the tether is reeled both out and in within a single orbit. Argatov and Silvennoinen [2010] showed that the orbits which allow for maximum energy efficiency have the shape of a "lying-eight" (∞) figure. More recently, Baayen and Ockels [2012], De Lellis et al. [2013], and Jehle and Schmehl [2014] have studied the *open-orbit* configuration, in which the tether reaches its maximum length after several orbits, at the end of the *traction* phase. Between two adjacent traction phases there is a *passive* phase, during which the cable is reeled back in. To this end, Fagiano [2009] proposed two maneuvers (Fig. 1):

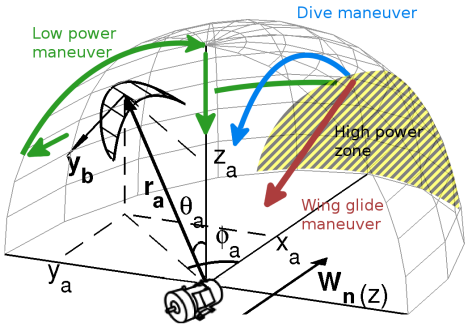

Fig. 1. Pumping kite, wind window, and reel-in maneuvers.

- the *wing glide maneuver* consists of orientating the kite with its lateral axis, $\mathbf{y_b}$, aligned upwind, similarly to a flag, while pulling the tether. This reduces the air drag on the kite, allowing it to be retrieved with only a small energy expense, even though the kite remains in the *high power zone*. The main drawback of this maneuver are implementation challenges to reorientate the kite, reliably, for the traction phase;
- the *low-power maneuver*, through which the tether is reeled-in while the kite is kept at the edge of the *wind window*, where the traction force is reduced. This maneuver requires a longer flight path, yielding a lower cycle power.

The main contribution of this work is the investigation of a *dive maneuver* that combines short duration with robustness, as an attempt to keep the angle of attack of the kite above a critical value in spite of wind turbulence.

The rest of the paper is organized as follows: Section 2 presents the kite model, followed by a robustness analysis in Section 3. A flight path reference is designed in Section 4, whereas simulation results with a tracking controller are discussed in Section 5. Section 6 concludes the paper.

⋆ This work was financially supported by CAPES, Brazil.
[1] there may be two tethers connecting the kite to the drum, depending on the concept.

Notation: $\|\mathbf{v}\|$ is the euclidean norm of a vector $\mathbf{v}$, its transpose is $\mathbf{v}'$, and its representation in the inertial and local frames is $(\cdot)_i$ and $(\cdot)_l$, respectively. The inner and cross product of two vectors are $\mathbf{v}_1 \bullet \mathbf{v}_2$ and $\mathbf{v}_1 \times \mathbf{v}_2$, whereas $|u|$, $\overline{u}$, $\underline{u}$, $\tilde{u}$ and $\hat{u}$ represent the magnitude, maximum, minimum, mean and equilibrium values of a scalar u. Vectors and scalars are continuous-time variables, if not otherwise stated. $\dot{(\cdot)}$, $\ddot{(\cdot)}$ and $\dddot{(\cdot)}$ are their 1st, 2nd and 3rd time-derivatives.

2. SYSTEM MODEL

The kite is modeled as a point-mass tethered to a fixed point on the ground, where both the origin of the *inertial frame* and the electric machine are located (Fig. 1). The kite position is $\mathbf{r_a} := r_a \left[\sin\theta_a \cos\phi_a \;\; \sin\theta_a \sin\phi_a \;\; \cos\theta_a\right]_i'$, where θ_a is the *complementary elevation* angle, ϕ_a is the *azimuth* angle, and r_a is the cable length. The tether attachment point at the kite is the origin of the *local frame*, defined by the vectors $\mathbf{e}_\theta := d\mathbf{r_a}/d\theta$, $\mathbf{e}_\phi := d\mathbf{r_a}/d\phi$, and $\mathbf{e_r} := d\mathbf{r_a}/dr$. The nominal wind, $\mathbf{W_n} := [W_n(z_a) \;\; 0 \;\; 0]_i'$, defines the $\mathbf{x}$ direction of the inertial frame, and depends on the flight altitude, z_a. The body frame is fixed to the airfoil, originated at the kite attachment point, and is composed by the orthonormal vectors $\mathbf{x_b}$, $\mathbf{y_b}$, and $\mathbf{z_b} = \mathbf{x_b} \times \mathbf{y_b}$. The orientation of $\mathbf{x_b}$ with respect to the tangent local plane, $(\mathbf{e}_\theta, \mathbf{e}_\phi)$, is represented by the *base angle of attack*, $\alpha_0 := \arccos(-\mathbf{e}_\theta \bullet \mathbf{x_b})$. We assume a pitch dynamics $\dot{\alpha}_0 := k_\alpha u_\alpha$, where u_α is the voltage applied to the pitch motor. With turbulence $\mathbf{W_t}$ in any direction, the resulting wind is $\mathbf{W_l} := \mathbf{W_n} + \mathbf{W_t}$. The *kite* velocity in the local frame is $\mathbf{W_a} := \left[r_a\dot{\theta}_a \;\; \sin\theta_a r_a \dot{\phi}_a \;\; \dot{r}_a\right]_l'$, and the *effective wind* is

$$\begin{aligned}\mathbf{W_e} &:= \mathcal{R}_i^l \mathbf{W_l} - \mathbf{W_a} \\ &= \begin{bmatrix}\cos\theta_a\cos\phi_a & \cos\theta_a\sin\phi_a & -\sin\theta_a \\ -\sin\phi_a & \cos\phi_a & 0 \\ \sin\theta_a\cos\phi_a & \sin\theta_a\sin\phi_a & \cos\theta_a\end{bmatrix}\begin{bmatrix}W_x \\ W_y \\ W_z\end{bmatrix}_i - \mathbf{W_a}\,,\end{aligned} \tag{1}$$

where $\mathcal{R}_i^l$ is the rotation matrix from the inertial to the local frame. We can now define a *wind frame*, composed by the orthonormal vectors $\mathbf{x_w} := -\mathbf{W_e}/\|\mathbf{W_e}\|$, which points opposite to the effective wind direction, and $\mathbf{z_w} := \mathbf{x_w} \times \mathbf{y_w}$. The definition of $\mathbf{y_w}$ can be found in Fagiano [2009] and Diehl [2001], where this model is derived from. Due to the kite position and velocity, the *total angle of attack* is

$$\alpha := \alpha_0 + \Delta\alpha = \alpha_0 + \arcsin\left(\frac{\mathbf{W_e} \bullet \mathbf{e_r}}{\|\mathbf{W_e}\|}\right). \tag{2}$$

Flight dynamics is determined by the following forces. The weight, $\mathbf{G} := (m + 0.5m_c)g\left[sin\theta_a \;\; 0 \;\; -\cos\theta_a\right]_l'$, acts upon the kite mass, m, and the cable mass, $m_c := 0.25\rho_c\pi d_c^2 r_a$, where ρ_c is the cable density, d_c is the cable diameter, and g is the gravity acceleration. The apparent forces (inertial and Coriolis) are $\mathbf{P} := [P_\theta \;\; P_\phi \;\; P_r]'$, with $P_\theta := m(\dot{\phi}_a^2 r_a \sin\theta_a\cos\theta_a - 2\dot{r}_a\dot{\theta}_a)$, $P_\phi := -2m\dot{\phi}_a(\dot{r}_a\sin\theta_a + r_a\dot{\theta}_a\cos\theta_a)$, and $P_r := mr_a(\dot{\theta}_a^2 + \dot{\phi}_a^2\sin^2\theta_a)$. The cable traction force is $\mathbf{T} := T\mathbf{e_r}$. The aerodynamic forces are: the *kite drag*, $\mathbf{D_a} := -0.5\rho A C_d(\alpha)\|\mathbf{W_e}\|^2\mathbf{x_w}$, where ρ is the air density, A is the kite characteristic area, and $C_d(\alpha)$ is the kite drag coefficient; the *cable drag*, $\mathbf{D_c} := -0.125\rho C_c r_a d_c \cos\Delta\alpha\|\mathbf{W_e}\|^2\mathbf{x_w}$, where C_c is a constant cable drag coefficient; and the *kite lift*, $\mathbf{L} := 0.5\rho A C_l(\alpha)\|\mathbf{W_e}\|^2\mathbf{z_w}$, where $C_l(\alpha)$ is the lift coefficient. Note that the drag forces are collinear with $\mathbf{W_e}$, whereas $\mathbf{L} \perp \mathbf{W_e}$. In Fig. 2 we present the aerodynamic coefficients, obtained from Ostowari and Naik [1984], for a NACA 4415 airfoil with infinite aspect ratio [2], ϵ. We will assume this aerodynamic behavior for our kite, even though a typical value would be $\epsilon = 6$. As ϵ decreases, the second peak on the lift curve tends to decrease and eventually disappear.

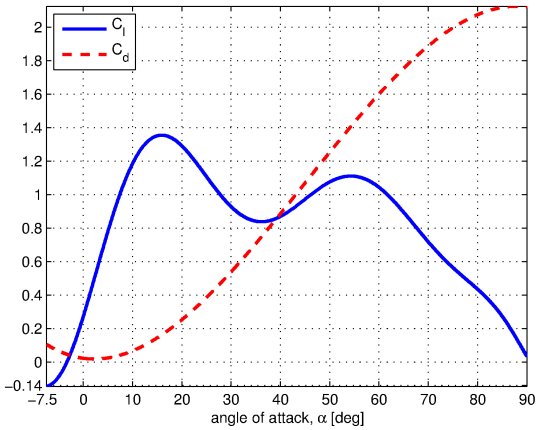

Fig. 2. Kite lift, $C_l(\alpha)$, and drag, $C_d(\alpha)$, coefficients.

The electric machine dynamics is $J\dot{\omega} := Tr_d + \tau_e$, where J is its moment of inertia, ω its angular speed, and r_d is the drum radius. In the passive phase the machine operates as a motor, and we model the electric torque as $\tau_e := -k_m u_e$, where k_m is a torque constant, and u_e is the voltage applied to the motor.

We define the control input vector $\mathbf{v} := [\psi \;\; u_\alpha \;\; u_e]'$, where ψ is the *roll angle*, which determines the projections of the aerodynamic forces in the local frame. With $\mathbf{\Gamma} := \mathbf{L}(\mathbf{q}, \psi, \mathbf{W_l}) + \mathbf{D_a}(\mathbf{q}, \psi, \mathbf{W_l}) + \mathbf{D_c}(\mathbf{q}, \mathbf{W_l})$ being the resulting aerodynamic force, and $\mathbf{q} := \left[\theta_a \;\; \phi_a \;\; r_a \;\; \dot{\theta}_a \;\; \dot{\phi}_a \;\; \dot{r}_a \;\; \alpha\right]'$ the state vector, the equations of motion of the system are

$$\begin{bmatrix} mr_a\ddot{\theta}_a \\ mr_a\sin\theta_a\ddot{\phi}_a \\ (m + J/r_d^2)\ddot{r}_a\end{bmatrix}_l = \mathbf{G} + \mathbf{P} + \mathbf{\Gamma}(\mathbf{q}, \psi, \mathbf{W_l}) - \begin{bmatrix} 0 \\ 0 \\ \frac{k_m}{r_d}u_e\end{bmatrix}, \tag{3}$$

with $\dot{q}_7 = \dot{\alpha} = k_\alpha u_\alpha + \dot{\Delta}\alpha$. We assume all states and the local wind, $\mathbf{W_l}$, are measured.

2.1 Longitudinal Model in the Downwind Plane

For the sake of analysis and control design simplification, we propose the *dive maneuver* in the downwind $(\mathbf{x}, \mathbf{z})_i$ plane, as depicted in Fig. 3. We assume the airfoil is kept at $\phi_a = 0°$ by a closed-loop controller that manipulates ψ, which is not in the scope of this work. Hence, defining $L := \|\mathbf{L}(\mathbf{x}, \mathbf{W_l})\|$, and $D := \|\mathbf{D_a}(\mathbf{x}, \mathbf{W_l})\| + \|\mathbf{D_c}(\mathbf{x}, \mathbf{W_l})\|$, the control vector as $\mathbf{u} := [u_\alpha \;\; u_e]'$, and the state vector as $\mathbf{x} := \left[\theta_a \;\; \dot{\theta}_a \;\; r_a \;\; \dot{r}_a \;\; \alpha\right]'$, the longitudinal downwind system

[2] refers to the ratio between wing length and width.

dynamics, in the local frame, can be represented in the state space as

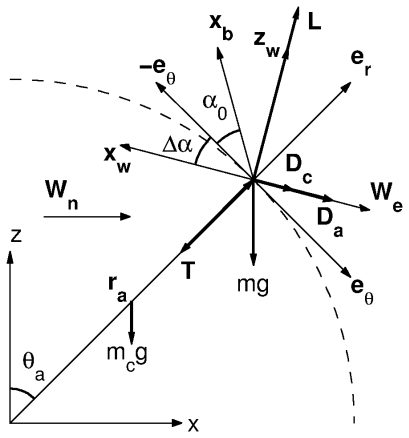

Fig. 3. Longitudinal downwind model definitions.

$$\begin{cases} \dot{x}_1 = x_2 \\ \dot{x}_2 = \dfrac{\beta_\theta}{x_3}\left[(\mathbf{G}+\mathbf{P})\bullet\mathbf{e}_\theta - L\sin\Delta\alpha + D\cos\Delta\alpha\right] \\ \dot{x}_3 = x_4 \\ \dot{x}_4 = \beta_r\left[(\mathbf{G}+\mathbf{P})\bullet\mathbf{e_r} + L\cos\Delta\alpha + D\sin\Delta\alpha - \beta_e u_e\right] \\ \dot{x}_5 = k_\alpha u_\alpha + \dot{\Delta}\alpha\,, \end{cases} \tag{4}$$

where $\beta_\theta := 1/m$, $\beta_r := 1/(m + J/r_d^2)$, and $\beta_e := k_m/r_d$.

We note that (4) is only valid if the tether is under positive tension, i.e.

$$T = (J/r_d^2)\ddot{r}_a + \beta_e u_e > 0\,. \tag{5}$$

If this is not satisfied, the cable becomes loose and control over the kite is lost.

3. ROBUSTNESS ANALYSIS

The stability of the pumping kite generator in the passive phase is more susceptible to wind disturbances than in the traction phase. This is because, in order to minimize the energy expense to reel in the cable, T needs to be small, and consequently α becomes small, close to a critical value, $\alpha_\diamond$, below which the kite may collapse due to aerodynamic effects not modeled herein. Hence a margin on the angle of attack, $\alpha - \alpha_\diamond > 0$, is necessary for a robust passive phase. Depending on how much $\mathbf{W_e}$ is composed by $\mathbf{W_n}$, this margin can be more or less susceptible to be altered by variations in the magnitude or direction of $\mathbf{W_l} = \mathbf{W_n} + \mathbf{W_t}$. With that in mind, we define the *robustness index* as

$$\sigma := \left(\|\mathbf{W_e}\|/\|\mathbf{W_n}\|\right)(\alpha - \alpha_\diamond)\,, \tag{6}$$

i.e., the ratio $\|\mathbf{W_e}\|/\|\mathbf{W_n}\|$ can amplify the margin of attack angle. Observe that, by imposing $\dot{\theta}_a < 0$ more negative, a greater $\|\mathbf{W_e}\|/\|\mathbf{W_n}\|$ is obtained and the needed α to sustain this angular motion becomes, generally, greater. As a consequence, the margin $\alpha - \alpha_\diamond$ tends to increase, and so does σ. On the other hand, if we reel in the tether faster, with $\dot{r}_a < 0$ more negative, although the said ratio increases, the margin of attack angle needed to maintain $\dot{\theta}_a$ constant decreases and, in general, the robustness index is reduced. To illustrate this behavior let us assume a passive phase with $\dot{\theta}_a = 0$. For the following numerical analysis we will consider $\alpha_\diamond = -2°$, $W_n = 10\,\mathrm{m/s}$, and a kite with mass $m = 7\,\mathrm{kg}$, whose characteristic area is $A = 16\,\mathrm{m}^2$. The cable diameter is $d_l = 5\,\mathrm{mm}$, of density $\rho_l = 970\,\mathrm{kg/m}^3$, drag coefficient $C_c = 1.2$, and length $r_a = 500\,\mathrm{m}$. The θ_a-equilibria of model (4), $\hat{\theta}_a$, as a function of α_0 and $\dot{r}_a$, are shown in Fig. 4. The equilibrium angle of attack, $\hat{\alpha}$, and σ, are additional information and refer only to $\hat{\theta}_a$ in the Main Stable Node Segment (MSNS), which spans up to $\hat{\theta}_a \to 90°$.

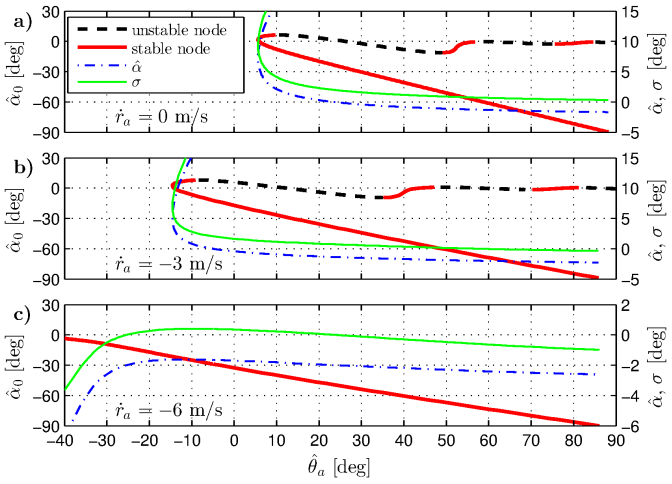

Fig. 4. Equilibria of θ_a as a function of α_0 and $\dot{r}_a$.

Considering the scenario with $\dot{r}_a = 0$ (Fig. 4a), by inspection in (2) we get that $\hat{\Delta}\alpha = \hat{\theta}_a$. Observe that, for high $\hat{\theta}_a$, the lift force, $\mathbf{L}$, is more aligned with the direction of $-\mathbf{e}_\theta$, and thus must have a lower magnitude. This requires a smaller α, and therefore σ diminishes. However, as $\hat{\theta}_a$ approaches the zenith point, $\mathbf{L}$ tends to become perpendicular to $\mathbf{e}_\theta$, hence a higher $\|\mathbf{L}\|$ is needed for the equilibrium, causing $\hat{\alpha}$ and σ to rapidly increase. The tether force follows this behavior. Note the existence of two $\hat{\alpha}_0$ for small equilibria inside the approximate interval $5° < \hat{\theta}_a < 10°$. By further increasing $\hat{\alpha}_0$ outside the MSNS the airfoil stalls, i.e. $\theta_a \to 90°$ with $T > 0$, due to an increase in the drag and a decrease in the lift caused by a high angle of attack.

Note that, as the unwinding speed is taken negative in Fig. 4b, the edge of the wind window, $\theta_a^\dagger = \min(\hat{\theta}_a)$, crosses the zenith point and reaches into negative values, whereas $\hat{\alpha}$, σ and $\hat{T}$ maintain the trend to increase as $\hat{\theta}_a \to \theta_a^\dagger$. However, if $\dot{r}_a$ is negative enough, as illustrated in Fig. 4c, $\hat{\alpha}$, σ and $\hat{T}$ fall as the wind window edge is approached. As a consequence, conditions $\alpha - \alpha_\diamond > 0$ and (5) are eventually violated. This inversion in the behavior occurs because, if $\theta_a \to \theta_a^\dagger$ with $\theta_a^\dagger < 0°$, the gravity forces start acting, along with $\mathbf{L}$, in the direction of $-\mathbf{e}_\theta$. The more negative $\dot{r}_a$ is, and consequently $\theta_a^\dagger$, the greater is the projection of the $\mathbf{G}$ onto $-\mathbf{e}_\theta$, requiring a progressively smaller $\|\mathbf{L}\|$, causing $\hat{\alpha}$, σ and T to decrease.

Even though $\sigma > 0$ for most of the equilibria in Fig. 4, the index may not be high enough to cope with the wind turbulence. A passive phase with a greater σ can be achieved by imposing $\dot{\theta}_a < 0$ to the kite while the cable is being retrieved, as illustrated in Fig. 5. Observe that, by making $\dot{\theta}_a$ faster, we can improve σ for a given $\dot{r}_a$ and θ_a. Nevertheless, a disadvantage of choosing $\dot{\theta}_a$ too negative is the increase in T, and consequently in the power consumption. Therefore a compromise between robustness and cycle power maximization has to be established. In Section 4.1 we will use (6) to determine reference values for $\dot{\theta}_a$ and $\dot{r}_a$ for the dive maneuver.

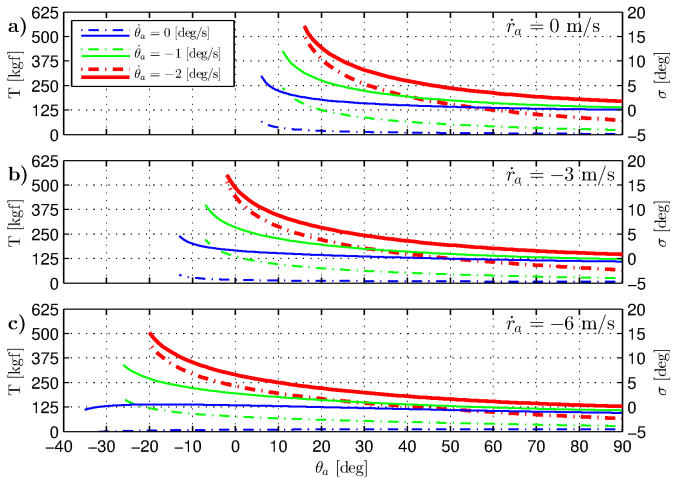

Fig. 5. $T(\textbf{-}\cdot)$ and $\sigma(\textbf{—})$ as a function of θ_a, given $\dot{\theta}_a$ and $\dot{r}_a$.

4. CONTROL DESIGN

4.1 Offline Generation of the Flight Path Reference

The flight trajectory in the proposed passive phase is determined by $\dot{\theta}_a(t)$ and $\dot{r}_a(t)$. Therefore we can find offline-calculated reference values, $\dot{\theta}_{\text{ref}}(t)$ and $\dot{r}_{\text{ref}}(t)$, that respect a desired robustness index, σ_{ref}, while maximize the cycle power,

$$P_{\text{cyc}} := \frac{\int_{t_0}^{t_1} P_{\text{t}}(\tau)d\tau + \int_{t_1}^{t_2} P_{\text{p}}(\tau)d\tau}{(t_1 - t_0) + (t_2 - t_1)}\,, \tag{7}$$

where $E_{\text{t}} := \int_{t_0}^{t_1} P_{\text{t}}(\tau)d\tau$ and $\Delta t_{\text{t}} := t_1 - t_0$ are the traction phase electric energy and duration, respectively, known *a priori*. The instantaneous electric power in the passive phase, of duration $\Delta t_{\text{p}} := t_2 - t_1$, is $P_{\text{p}}(t) := T(\theta_a, \dot{\theta}_a, r_a, \dot{r}_a, t)\dot{r}_a(t)/\eta$, where $0 < \eta < 1$ is the overall efficiency in converting electric to mechanical power.

Given the complexity in finding an analytical, continuous-time solution to this problem, our approach was to work in a discrete domain, i.e. with vectors of known resolution and size. Because we do not know Δt_{p}, we choose not to work with a discrete-time domain. Instead, given that the system equilibria depend more strongly on θ_a than on r_a, we specify the optimization domain as $\vartheta = \{\vartheta[i] \in \mathbb{R} : \vartheta[i] := \overline{\theta}_a - \delta\vartheta(i-1);\ i = 1, \ldots, p\}$, where $0 < \overline{\theta}_a < 90°$ occurs at the beginning of the passive phase, $\delta\vartheta > 0$ is the domain resolution, and $p > 1$ is the domain vector size. The idea is to make the optimizer apply a reference pair $(\dot{\theta}_a, \dot{r}_a)_{\text{ref}}[i]$ to the system as long as θ_a is in the i-th slot, i.e. $\vartheta[i] \le \theta_a < \vartheta[i+1]$. Thus, we approximate the electric energy spent in the passive phase as

$$E_{\text{p}} := \int_{t_1}^{t_2} P_{\text{p}}(\tau)d\tau \approx (1/\eta)\sum_{i=1}^{n} \mathsf{T}[i]\dot{r}_a[i]\delta t[i]\,, \tag{8}$$

where n corresponds to the slot in which the passive phase ends, characterized by $r_a \le \underline{r}_a = \overline{r}_a - \Delta r_a$, with $\Delta r_a > 0$ being the amount of tether to reel in. The duration of each slot is defined as

$$\delta t[i] = \begin{cases} \dfrac{\delta\vartheta}{\dot{\theta}_{\text{ref}}[i]} & \text{if } r_a[i] + \dot{r}_{\text{ref}}[i]\dfrac{\delta\vartheta}{\dot{\theta}_{\text{ref}}[i]} > \underline{r}_a \\ \dfrac{\underline{r}_a - r_a[i]}{\dot{r}_{\text{ref}}[i]} & \text{else}\,. \end{cases} \tag{9}$$

The *if*-condition in (9) means that $\vartheta[i+1]$ will be needed to complete the passive phase, else the integration stops at $i = n$. To calculate $T[i] = T\big(\vartheta[i], r_a[i], (\dot{\theta}_a, \dot{r}_a)_{\text{ref}}[i]\big)\big)$, we define the tether length of each slot as $r_a[i] := r_a[i-1] + \dot{r}_{\text{ref}}[i-1](\delta\vartheta/\dot{\theta}_{\text{ref}}[i-1])$.

Preliminary optimization tests with an unconstrained trajectory showed that the solutions presented a higher $|\dot{\theta}_a|$ and a lower $|\dot{r}_a|$ in the beginning of the passive phase, changing approximately linearly to lower $|\dot{\theta}_a|$ and higher $|\dot{r}_a|$. Nevertheless, for high enough σ_{ref}, reference values between adjacent slots could vary abruptly in magnitude and direction. This is undesired, since it poses a challenge to the tracking controller, specially in terms of avoiding an undershoot in the angle of attack below $\alpha_\diamond$ when slowing down $\dot{\theta}_a$. Hence, aiming at a monotonically, smooth variation of the reference pair, we constrain the $\dot{\theta}_{\text{ref}}[i], \dot{r}_{\text{ref}}[i]$ trajectories to straight lines (in the ϑ-domain), establishing the optimization solution, $\Omega = (\gamma_\theta, \mu_\theta, \gamma_r, \mu_r)$, as the coefficients of such linear curves

$$\begin{aligned} \dot{\theta}_a[i] &= \gamma_\theta + \mu_\theta(\overline{\theta}_a - \vartheta[i]) \\ \dot{r}_a[i] &= \gamma_r + \mu_r(\overline{\theta}_a - \vartheta[i])\,. \end{aligned} \tag{10}$$

We highlight that these constrained trajectories showed similar P_{cyc} values as the unconstrained ones.

During the maneuver, the instantaneous references can be determined by replacing ϑ by θ_a and $[i]$ by (t) in (10). With the definitions above, we can state the optimization problem as

$$\begin{aligned} \Omega = \arg \max_{\dot{\theta}_a[i], \dot{r}_a[i]} & \left(\frac{E_{\text{t}} + \eta\sum_{i=1}^{n} T[i]\dot{r}_a[i]\delta t[i]}{\Delta t_{\text{t}} + \sum_{i=1}^{n}\delta t[i]}\right) \\ \text{such that} & \\ \sigma \ge \sigma_{\text{ref}} & \\ 0 < P_{\text{cyc}} < \tilde{P}_{\text{t}}\,, & \end{aligned} \tag{11}$$

where the constraint $0 < P_{\text{cyc}} < \tilde{P}_{\text{t}}$ is added to reduce the search domain, helping the algorithm to converge.

4.2 Reference Tracking Control

Differently from Fagiano [2009], we designed our passive phase maneuver considering we can manipulate α_0 and taking into account the electric motor/winch dynamics. Hence we have a square system with output vector $\mathbf{y} = \begin{bmatrix}\dot{\theta}_a & \dot{r}_a\end{bmatrix}'$ and input vector $\mathbf{u} = [u_\alpha \; u_e]'$. Given the highly nonlinear behavior of this system, and the fact that its outputs are coupled, we used a static, locally regular state-feedback control law in the form $\mathbf{u} = \mathtt{a}(\mathbf{x}) + \mathtt{b}(\mathbf{x})\mathbf{v}$. According to Isidori [1995], it yields a decoupled, linear system with same outputs, but a new input vector $\mathbf{v}$, which is used for stabilization and reference tracking. Due to space limitations, details on this controller are being published in another paper.

5. SIMULATION RESULTS

To test the robustness of our passive phase, we use the *Dryden* wind turbulence model (see e.g. Cook [2013]). It creates turbulence as a stochastic process by applying band-limited white noise through digital filters. RMS-turbulence intensity, $\zeta(z_a)$, for $z_a < 304.8\,\mathrm{m}$ (1000 ft), is defined in the longitudinal (lo) and vertical (ve) components as

$$\zeta_{\mathrm{ve}} := 0.1 W_{20} = \mu W_n \tag{12a}$$

$$\zeta_{\mathrm{lo}} := \frac{1}{(0.177 + 0.0027 z_a)^{0.4}} \zeta_{\mathrm{ve}}\,, \tag{12b}$$

where W_{20} is the wind speed at 20 ft. Note that $\zeta_{\mathrm{lo}} \geq \zeta_{\mathrm{ve}}$. Although the kite may reach $z_a > 304.8\,\mathrm{m}$, for the sake of simplicity, we will remain with this model as a worst-case turbulence scenario. We will also assume a constant nominal wind speed, $W_n(z_a) = 10\,\mathrm{m/s}\;\forall z_a > 0$, and hence define ζ_{ve} in (12) in terms of a factor, $\mu > 0$, of W_n. This way we can check how much turbulence is endured by the system without violating either of the stop conditions

$$\text{a) } \alpha > \alpha_\diamond,\ \text{b) } T > 0,\ \text{c) } \theta_a < 90^\circ\,. \tag{13}$$

Condition (13a) means that the kite does not collapse, (13b) refers to (5), guaranteeing that model (4) remains valid, and (13c) checks for a collision with the ground.

To optimize the dive maneuver, it was considered $\Delta r_a = 100\,\mathrm{m}$, and a traction phase with $\tilde{P}_{\mathrm{t}} = 15\,\mathrm{kW}$ and $\dot{r}_{a,\mathrm{p}} = 2\,\mathrm{m/s}$. Other parameters were set as $r_d = 0.3\,\mathrm{m}$, $J = 2.25\,\mathrm{kg\,m^2}$, $k_m = 2\,\mathrm{Nm/V}$, and $k_\alpha = 0.3\,\mathrm{deg(sV)^{-1}}$. The domain resolution was $\delta\vartheta = 2.5\,\mathrm{deg}$. Table 1 contains some optimization and simulation results as a function of a critical angle of attack, $\alpha_\diamond$, and a desired robustness margin, σ_{ref}. The cycle power calculated by the optimizer is P_{cyc}, which accounts for an efficiency of $\eta = 0.8$. The $\dot{\theta}_{\mathrm{ref}}$ and $\dot{r}_{\mathrm{ref}}$ columns contain the initial and final values of the references. The solution components are limited to the intervals $\gamma_\theta \in [-8, -0.1]$ deg/s, $\mu_\theta \in [0, 0.6]\ \mathrm{s}^{-1}$, $\gamma_r \in [-6, -0.1]$ m/s, and $\mu_r \in [-0.6, 0]\ \mathrm{m\,(s\,deg)^{-1}}$. The passive phase is assumed to start at $\overline{\theta}_a = 70^\circ$, and finishes at $\underline{\theta}_a$ after a time interval Δt_{p}. The amount of admissible perturbation is indicated by $\mu^\dagger$, which corresponds to the highest μ in (12) for which 20 maneuvers [3] could be completed, with at most 1 failure, with respect to the stop conditions (13). $\|\overline{\mathbf{W_t}}\|$ indicates the maximum turbulence intensity registered during these completed simulations.

$\alpha_\diamond$	σ_{ref}	P_{cyc}	$\dot{\theta}_{\mathrm{ref}}$	$\dot{r}_{\mathrm{ref}}$	$\underline{\theta}_a$	Δt_{p}	$\mu^\dagger$	$\|\overline{\mathbf{W_t}}\|$
[deg]		[kW]	[deg/s]	[m/s]	[deg]	[s]	[%]	[m/s]
−3	1	10.9	$-(0.4, 0.4)$	$-(6.0, 6.0)$	64	17	3	1.1
	2	10.5	$-(1.2, 1.2)$	$-(6.0, 6.0)$	50	17	6	1.9
	3	10.0	$-(1.8, 1.7)$	$-(6.0, 6.0)$	41	17	8	3.2
	4	9.4	$-(2.3, 2.1)$	$-(6.0, 6.0)$	34	17	10	3.8
	5	8.7	$-(2.7, 2.4)$	$-(6.0, 6.0)$	28	17	12	4.7
	6	8	$-(3.1, 2.6)$	$-(6.0, 6.0)$	22	17	12	5.9
	7	7.2	$-(3.3, 2.7)$	$-(5.0, 6.0)$	15	18	14	6.0
	8	6.5	$-(3.5, 2.6)$	$-(3.9, 5.7)$	7	21	16	7.8
	9	5.8	$-(3.5, 2.1)$	$-(2.0, 5.1)$	−6	28	20	6.4
−2	1	9.5	$-(2.0, 2.0)$	$-(5.6, 6.0)$	35	17	2	1.1
	2	8.8	$-(2.7, 2.2)$	$-(5.6, 6.0)$	28	17	5	2.7
	3	7.9	$-(2.9, 2.4)$	$-(4.2, 6.0)$	18	20	6	3.0
	4	7.1	$-(3.1, 2.1)$	$-(3.0, 5.3)$	7	24	8	4.5
	5	6.4	$-(3.3, 1.7)$	$-(1.8, 4.7)$	−3	30	9	5.3
	6	5.9	$-(3.4, 1.3)$	$-(0.5, 4.4)$	−11	37	11	6.1

Table 1. Dive maneuver optimization

Observe in Table 1 that indeed the system tends to endure more turbulence, both in terms of $\mu^\dagger$ and $\|\overline{\mathbf{W_t}}\|$, when more robustness, σ_{ref}, is required. Also, as $\alpha_\diamond$ is increased, less turbulence is endured by the system for a same σ_{ref}. On the other hand, the cycle power obtained by the optimizer, P_{cyc}, has an opposite behavior. This occurs because, if one wants more robustness, a higher combination of attack angle (α) and effective wind magnitude ($\|\mathbf{W_e}\|$) is needed, according to (6). As a consequence, T increases, and so does the energy expense in the passive phase. It is also noteworthy that, as $\alpha_\diamond$ and σ_{ref} increase, the maneuver ends at a lower $\underline{\theta}_a$, eventually even crossing the zenith point, and takes more time. This longer duration also reduces the cycle power, according to (7). During the simulations, we recorded that the cycle power obtained with and without turbulence were close to P_{cyc}.

We note that, for higher σ_{ref}, the optimized trajectories take the kite closer to the edge of the wind window ($\theta_a^\dagger$), where the tracking controller is subject to singularity, which can easily be induced by turbulence. To avoid this issue, we reel-in the tether faster as the offline optimized value. This causes $\theta_a^\dagger < 0^\circ$ to decrease, and unfortunately also σ (see Fig. 5), rendering the system less robust to perturbations. That is why no results for higher σ_{ref} are shown in Table 1. Other strategies to avoid singularity without affecting σ are being investigated.

Simulation results of a single maneuver with $(\alpha_\diamond, \sigma_{\mathrm{ref}}) = (-2^\circ, 6^\circ)$ are presented in Fig. 6. The robustness index, which with $\mathbf{W_t} = 0$ is kept always above σ_{ref}, due to turbulence reached peaks of approximately 3°. The cycle power obtained was approximately 6.3 kW, and the passive phase lasted for 36 s, values close to those in Table 1. If the maneuver is simulated a high enough number of times, average values of cycle power and duration get closer to the optimized ones.

[3] The seeds of the deterministic and stochastic Dryden model are reshuffled before every simulation, in order to reproduce different scenarios of wind turbulence.

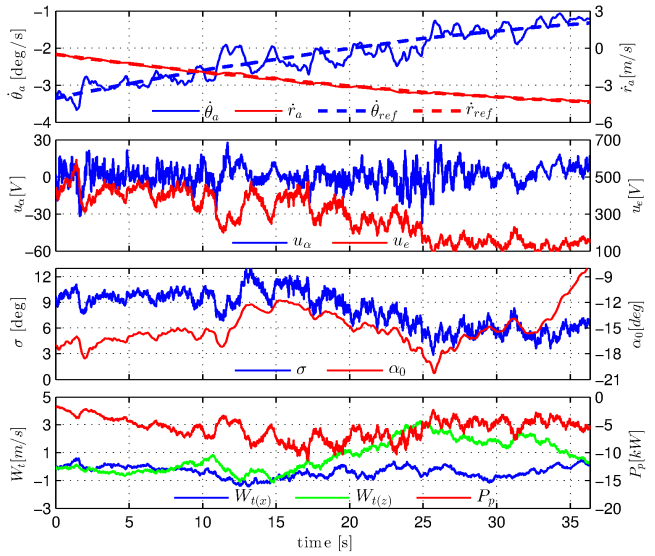

Fig. 6. Dive maneuver simulation under turbulent wind.

In Fig. 7 we illustrate how the maneuver path changes, depending on σ_{ref}, for $\alpha_\diamond = -2°$, without turbulence.

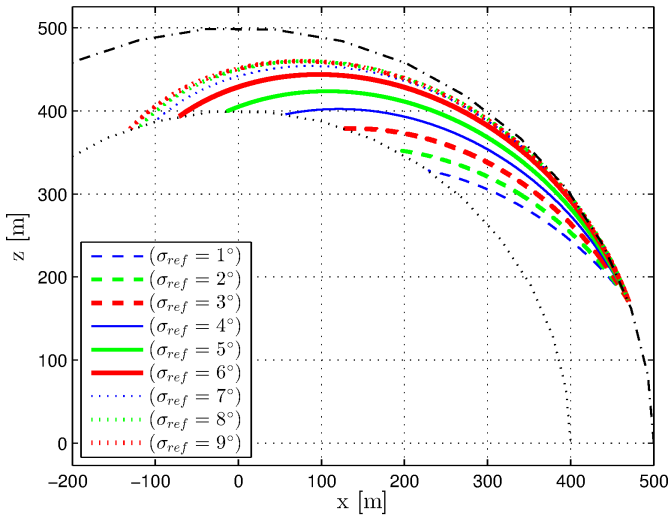

Fig. 7. Dive maneuver paths with $\alpha_\diamond = -2°$ and $\mathbf{W_t} = 0$.

6. FINAL REMARKS

This work dealt with the design of a robust passive phase for a pumping kite generator. As contributions, a robustness index was proposed, which quantifies how susceptible the airfoil angle of attack is to fall under a critical value. This is an important feature in the analysis of the practical feasibility of the passive phase for power kites. Also, an offline optimization of the flight trajectory was carried out to meet the compromise between robustness and cycle power maximization. It became evident that kites should be designed to operate at low attack angles, in order to allow for greater cycle power and robustness.

The optimization results found depend on the lift and drag coefficient curves, which in practice might be different than the ones considered. Therefore the intervals of critical attack angles and the trajectories obtained may vary accordingly. Also, the amount of admissible perturbation depends on how fast the response of the pitch actuator and ground motor are, as well as on the control dynamics.

As future work, a passive phase with $\phi_a \neq 0$ and nominal wind that varies with altitude is to be investigated. Also, another strategy for dealing with the tracking control singularity without affecting the robustness index is desirable. Finally, an approach for measuring the effective wind and angle of attack is to be developed to allow the dive maneuver to be tested on a prototype.

7. ACKNOWLEDGMENTS

The authors would like to thank Hector B. Silveira for valuable support on the tracking controller design.

REFERENCES

M. Ahmed, A. Hably, and S. Bacha. High Altitude Wind Power Systems: A Survey on Flexible Power Kites. In *20th International Conference on Electrical Machines*, pages 2083–2089, Marseille, France, September 2012.

U. Ahrens, M. Diehl, and R. Schmehl, editors. *Airborne Wind Energy*. Green Energy and Technology. Springer Berlin Heidelberg, Berlin, Heidelberg, 2013.

C. L. Archer, L. Delle Monache, and D. L. Rife. Airborne wind energy: Optimal locations and variability. *Renewable Energy*, 64:180–186, April 2014.

I. Argatov and R. Silvennoinen. Energy conversion efficiency of the pumping kite wind generator. *Renewable Energy*, 35:1052–1060, 2010.

J. H. Baayen and W. J. Ockels. Tracking control with adaption of kites. *IET Control Theory & Applications*, 6:1–20, 2012.

M. V. Cook. *Flight Dynamics Principles: A Linear Systems Approach to Aircraft Stability and Control*. Butterworth-Heinemann, 3rd edition, 2013.

M. De Lellis, R. Saraiva, and A. Trofino. Turning angle control of power kites for wind energy. In *52nd IEEE Conference on Decision and Control*, pages 3493–3498, Firenze, Italy, December 2013. IEEE.

M. Diehl. *Real-Time Optimization for Large Scale Nonlinear Processes*. PhD thesis, Ruprecht-Karls-Universität, Heidelberg, Germany, 2001.

L. Fagiano. *Control of Tethered Airfoils for High-Altitude Wind Energy Generation*. PhD thesis, Politecnico di Torino, Torino, Italy, 2009.

B. Houska and M. Diehl. Optimal control for power generating kites. In *European Control Conference*, page 14, 2007.

International Energy Agency. World Energy Outlook 2012. Paris, France, 2012.

A. Isidori. *Nonlinear Control Systems*. Springer, 3rd edition, 1995.

C. Jehle and R. Schmehl. Applied Tracking Control for Kite Power Systems. *Journal of Guidance, Control, and Dynamics*, pages 1–12, February 2014.

C. Ostowari and D. Naik. Post Stall Studies of Untwisted Varying Aspect Ratio Blades with an NACA 4415 Airfoil Section – Part I. *Wind Engineering*, 8:176–194, 1984.